Inorg. Chem. **2008**, *47*, 11738−11744

Application of Electron Microscopy in the Observation of Technetium and Technetium Dioxide Nanostructures

G. W. Chinthaka Silva, Frederic Poineau, Longzhou Ma, and Kenneth R. Czerwinski*

University of Nevada, Las Vegas, Harry Reid Center for Environmental Studies, Box 454009, 4505 Maryland Parkway, Las Vegas, Nevada 89154

Received August 3, 2008

Transmission electron microscopy (TEM) was applied to characterize the microstructure of Tc metal and technetium dioxide synthesized by the decomposition of NH_4TcO_4. The morphology of the Tc metal and well-resolved TcO_2 particles were characterized using bright-field TEM and scanning TEM modes. Structural characterization of these two samples using high-resolution (HR) TEM was successfully performed for the first time on the nanoscale. The morphology of Tc metal showed significant differences when compared to TcO_2. The crystal structure of Tc metal on the nanoscale was shown to contain well-resolved lattice fringes without any defects. Because of the deficiency in point resolution, however, the two-dimensional structure details of Tc metal could not be observed as expected. On the other hand, structural details of TcO_2 were prominent at high resolution. With a 2-fold multiplicity in both directions, TcO_2 showed a unique atomic distribution corresponding to a monoclinic unit cell. Furthermore, the lattice parameters of the samples were refined by the Rietveld analysis of the powder X-ray diffraction patterns and were estimated by HRTEM. In the case of technetium dioxide, the stoichiometry was approximated to be $TcO_{2.3}$ using quantitative analysis of X-ray energy dispersive spectrometry. Electron energy-loss spectrometry verified the chemical phase of the two samples by their different chemical environments based on an energy shift of 2.0 eV of the N_{23} edge between TcO_2 and Tc metal.

1. Introduction

The isotope technetium-99 ($t_{1/2}$ = 213 000 y, β^- = 292 keV) is a high-yield fission product in light-water reactors. In the spent fuel, Tc is present as a metallic inclusion, forming an individual phase.[1−3] The proposed U.S. Department of Energy reprocessing process (UREX+) was designed to treat light-water-reactor spent fuel to recycle the actinides and partition the fission products for efficient disposal. The UREX process is a suite of aqueous-based solvent extraction processes that separate spent fuel into actinide materials for recycle and fission product components for the preparation of disposal waste forms. Uranium and technetium are extracted from the dissolved fuel during the first step (UREX segment). In the second step, Tc is removed from the U/Tc product and converted into a disposable waste form.[4,5] The ultimate waste form can be a metal or Tc alloy, and the Zr from cladding hulls is proposed as the additional metallic component. Transmutation or incineration of ^{99}Tc has its own difficulties due to large reactor capability requirements.[6] However, the metal produced as a transmutation target can be used as a potential waste form.[3] In a storage plant with oxidizing conditions, Tc metal could be partially oxidized to TcO_2. The release of ^{99}Tc into the environment will then be dependent on the solubility of technetium dioxide. In this context, understanding the structure and properties of Tc metal and technetium dioxide is important in order to predict their long-term behavior in storage conditions, whether the waste form is a single metal or an alloy.

There are a number of studies that have been published on the structure of Tc metal and TcO_2. Lattice parameters

* Author to whom correspondence should be addressed. Phone: (702) 895 0501. Fax: (702) 895 3094. E-mail: czerwin2@unlv.nevada.edu.

(1) Rard, J. A. *J. Nucl. Radiochem. Sci.* **2005**, *6*, 197.
(2) Zilberman, B. Ya.; Pokhitonov, Yu. A.; Kirshin, M. Yu.; Ozawa, M.; Blokhin, A. A. *Radiochemistry (New York)* **2007**, *49*, 156.
(3) Ackerman, J. P. *Ind. Eng. Chem. Res.* **1991**, *30*, 141.
(4) Poineau, F.; Mazaubrun, J. Du.; Ford, D.; Fortner, J.; Kropf, J.; Smith, N.; Silva, C.; Long, K.; Jarvinen, G.; Czerwinski, K. *Radiochim. Acta* **xx**, xx In press.
(5) Vandegrift, G. F.; Regalbuto, M. C.; Aase, S. B.; Arafat, H. A.; Bakel, A. J.; Bowers, D. L.; Byrnes, J. P.; Clark, M. A.; Emery, J. W.; Falkenberg, J. R.; Gelis, A. V.; Hafenrichter, L. D.; Leonard, R. A.; Pereira, C.; Quigley, K. J.; Tsai, Y.; Vander Pol, M. J. *Proceedings of WM-04*, Tucson, AZ, February−March 2004.
(6) Kitamoto, A.; Setiawan, M. B. *Prog. Nucl. Energy* **2002**, *40*, 465.

10.1021/ic8014628 CCC: $40.75
Published on Web 11/18/2008

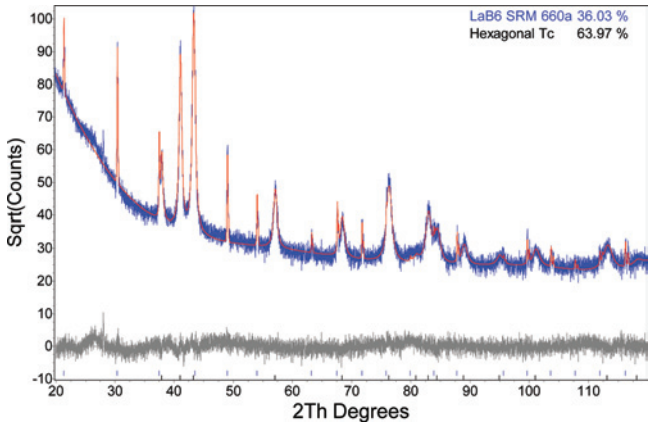

Figure 1. Rietveld analysis (Rwp = 8.1%) of the X-ray powder diffraction pattern of Tc metal.

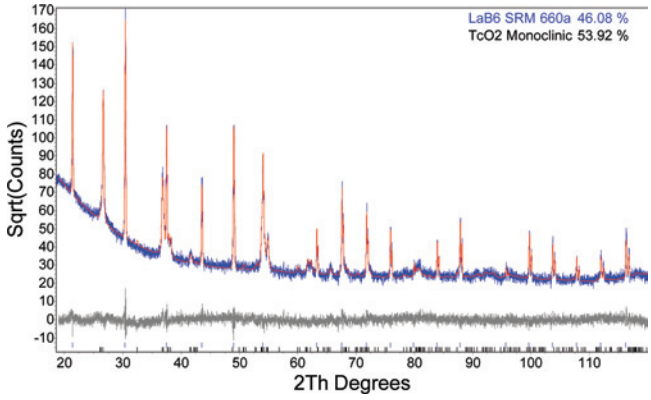

Figure 2. Rietveld analysis (Rwp = 9.5%) of the synthesized TcO_2.

and bond distances in technetium dioxide and Tc metal have been characterized by X-ray powder diffraction (XRD), neutron powder diffraction, and X-ray absorption fine structure.[7−9] However, characterization by microscopic techniques such as transmission electron microscopy (TEM) is not well-developed, and only a few publications on the microscopic characterization of Tc materials are documented.[10−12] Therefore, in order to provide a complete understanding of these materials, it is important to perform morphological and microstructural characterizations. Furthermore, transmission electron microscopy is a robust technique for morphological and microstructural characterizations. One of the powerful TEM modes, high-resolution TEM (HRTEM), together with Bloch Wave HRTEM presentations can be used to obtain the spatial arrangements of

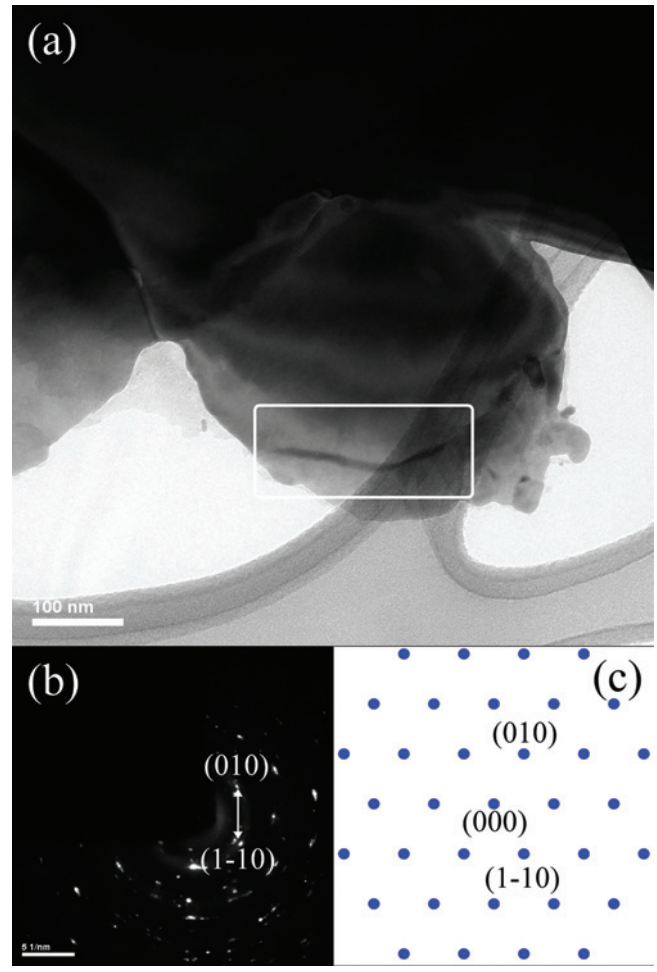

Figure 3. TEM BF image of the Tc metal sample (a) together with the experimental (b) and simulated SAD patterns (c) in the [001] zone axis.

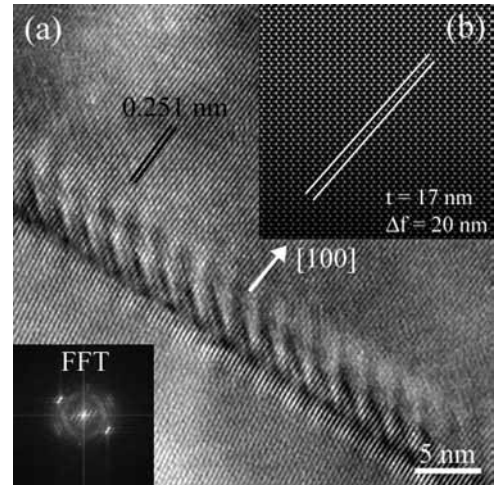

Figure 4. Experimental HRTEM image (a) and the Bloch wave presentation of the calculated HRTEM image (b) along the [100] direction under [001] beam direction. Thickness (*t*) and defocus values (*f*) used in the HRTEM simulation are 17 and 20 nm, respectively.

atoms in a material.[13] TEM techniques can also be used to interpret the morphology of radioactive materials such as

(7) Almahamid, I.; Bryan, J. C.; Bucher, J. J.; Burrell, A. K.; Edelstein, N. M.; Hudson, E. A.; Kaltsoyannis, N.; Lukens, W. W.; Shuh, D. K.; Nitsche, H.; Reich, T. *Inorg. Chem.* **1995**, *34*, 193.
(8) Muller, O.; White, W. B.; Roy, R. J. *Inorg. Nucl. Chem.* **1964**, *26*, 2075.
(9) Rodriguez, E. E.; Poineau, F.; Llobet, A.; Sattelberger, A. P.; Bhattacharjee, J.; Waghmare, U. V.; Hartmann, T.; Cheetham, A. K. *J. Am. Chem. Soc.* **2007**, *129*, 10244.
(10) Yamamura, T.; Yubuta, K.; Satoh, I.; Yoshida, Y.; Shiokawa, Y.; Sekine, T.; Sugiyama, W.; Park, K. C.; Tomiyasu, H. *J. Supercrit. Fluids* **2007**, *43*, 317.
(11) Zachara, J. M.; Heald, S. M.; Jeon, B. H.; Kukkadapu, R. K.; Liu, C.; McKinley, J. P.; Dohnalkova, A. C.; Moore, D. A. *Geochim. Cosmochim. Acta* **2007**, *71*, 2137.
(12) Sekine, T.; Narushima, H.; Kino, Y.; Kudo, H.; Lin, M.; Katsumura, Y. *Radiochim. Acta* **2002**, *90*, 611.
(13) Meyer, R. R.; Sloan, J.; Dunin-Borkowski, R. E.; Kirkland, A. I.; Novotny, M. C.; Bailey, S. R.; Hutchison, J. L.; Green, M. L. H. *Science* **2000**, *289*, 1324.

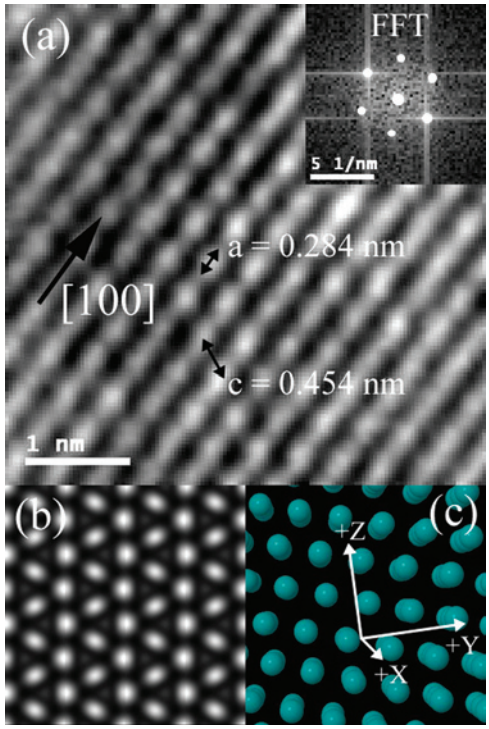

Figure 5. Magnified HRTEM image of Tc metal particle (a) and the calculated HRTEM image (b) along the [100] direction and [001] beam direction using $t = 15$ nm and $\Delta f = 20$ nm. Part c shows the spatial orientation of the Tc-metal modeled in the [100] direction.

uranium nitrides and actinide-bearing waste forms.[14−16] Some of the TEM modes are also found to be applicable in studying the radiation tolerance of different structures.[17,18]

An insight into the chemical and crystal structures of these two materials using microscopy is provided in this effort. TEM was applied to examine the morphology and microstructure of metallic Tc and its oxide (TcO_2) synthesized by the thermal decomposition of NH_4TcO_4. The morphology of these two samples was characterized using bright field (TEM BF) and scanning (STEM) modes. HRTEM was used for the first time on these two materials, and electron energy-loss spectrometry (EELS) was also utilized to confirm the different chemical environments. X-ray energy dispersive spectrometry (XEDS) measurements were performed qualitatively to infer the purity of the two samples. Quantitative measurement by XEDS was also used to verify the stoichiometry of TcO_2.

2. Experimental Details

2.1. Synthesis of Powder Samples. NH_4TcO_4 was purchased from Oak Ridge National Laboratory. The compound contains a black impurity, and therefore prior to use, the compound was purified by treatment with an ammoniac/hydrogen peroxide solution followed by evaporation to dryness.

2.1.1. Synthesis of TcO_2. Technetium dioxide was synthesized by thermal decomposition of NH_4TcO_4 at 700 °C under an inert atmosphere. A 425 mg sample of NH_4TcO_4 was transferred into a fused quartz boat and placed in a quartz tube situated in a tube

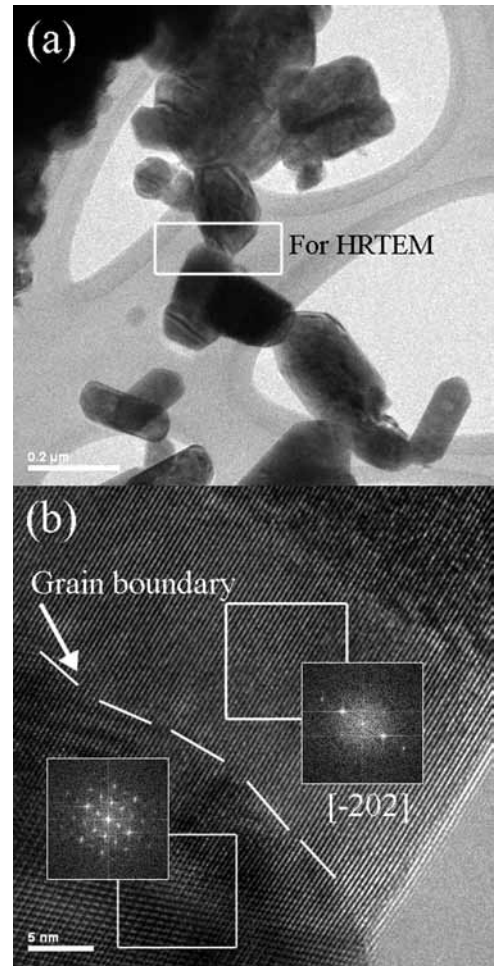

Figure 6. TEM images of TcO_2 in the BF mode (a) and in the high-resolution mode (b).

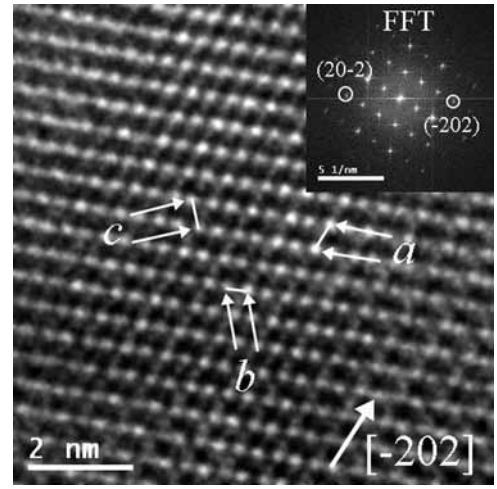

Figure 7. Magnified HRTEM image of the TcO_2 along the [−202] direction under the [010] beam direction.

(14) Silva, G. W. C.; Yeamans, C. B.; Ma, L.; Cerefice, G. S.; Czerwinski, K. R.; Sattelberger, A. P. *Chem. Mater.* **2008**, *20*, 3076.
(15) Fortner, J. A.; Buck, E. C.; Ellison, A. J. G.; Bates, J. K. *Ultramicroscopy* **1997**, *67*, 77.
(16) Nogita, K.; Une, K. *J. Nucl. Mater.* **1997**, *250*, 244.
(17) Sickafus, K. E.; Minervini, L.; Grimes, R. W.; Valdez, J. A.; Ishimaru, M.; McClellan, F; Li, K. J.; Hartmann, T. *Science* **2000**, *289*, 748.
(18) Sykora, R. E.; Raison, P. E.; Haire, R. G. *J. Solid State Chem.* **2005**, *178*, 578.

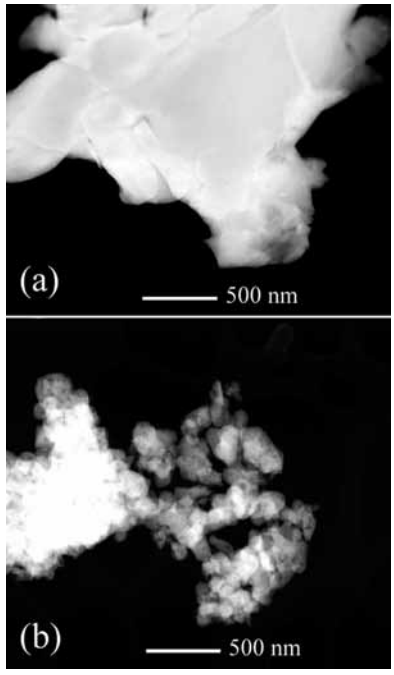

Figure 8. STEM images of Tc metal and TcO_2 samples.

furnace. The quartz tube was flushed with argon for 1 h, and the furnace was set to 350 °C with a ramp rate of 5 °C/min. The furnace was set to 350 °C for 1 h and then heated to 700 °C with a ramp rate of 5 °C/min. The 700 °C temperature was maintained for 2 h in order to complete the reaction and to crytallize the produced TcO_2. The reaction yielded 282 mg of TcO_2.

2.1.2. Synthesis of Tc Metal. Technetium metal was synthesized by steam-reforming thermal reduction of TcO_2 at 910 °C under a wet argon atmosphere in the presence of activated carbon. A 218.0 mg sample of NH_4TcO_4 was transferred into a fused quartz boat and placed in a quartz tube situated in a tube furnace. The quartz tube was flushed for 1.5 h with ultra-high-purity argon, and the furnace was set to 300 °C with a ramping rate of 20 °C/min. The furnace was set to 300 °C for 1 h and heated to 910 °C with a ramping rate of 20 °C/min. The 910 °C conditions were held for 1 h, resulting in the recovery of 17.0 mg of Tc metal.

2.2. Characterization Methods. 2.2.1. XRD Analysis. XRD patterns were obtained at the Department of Geoscience of the University of Nevada, Las Vegas, using a Philips PANalytical X'Pert Pro instrument with a Cu Kα target and a Ni filter, using a 40 mA current and 40 kV tension. Rietveld analyses on these XRD patterns together with an internal standard (LaB6 SRM 660a) were performed in order to refine the lattice parameters.

2.2.2. Microscopy. The Tc samples for TEM analysis were prepared by the solution-drop method. The samples were ground in a mortar to microsized particles and mixed with ethanol. One drop of the solution was added onto a 3-mm-diameter carbon film supported on a copper grid which was used as the sample holder.

TEM imaging was performed using a TECNAI-G2-F30 Spertwin transmission electron microscope with a 300 keV field emission gun. The conventional diffraction contrast mode, which is known as the bright-field mode (TEM BF), was used to study the morphology of the samples. Further characterization was performed using the HRTEM mode. TEM images were recorded using a slow-scan CCD camera attached on a Gatan GIF 2000 (Gatan Image Filter). Microstructure characterization at high resolution was done using HRTEM images together with the experimental selected area electron diffraction patterns (SAD). Furthermore, SAD and HRTEM simulations[19] were employed to confirm the experimental micrographs. STEM and the corresponding XEDS were exploited to study the elemental distributions of the samples. The bonding characteristics of Tc metal and TcO_2 were confirmed by EELS.

3. Results

3.1. X-Ray Powder Diffraction Analysis of the Samples. The experimental X-ray powder diffraction pattern for Tc metal is shown in Figure 1 together with the calculated pattern (red color) determined assuming the Tc-hexagonal pattern (ICSD # 52498). The lattice parameters acquired by Rietveld analysis are a (b) = 2.7431(3) Å, c = 4.3989 (5) Å, and c/a = 1.603. These values have a good agreement with the a (b) = 2.743 (1) Å, c = 4.400 (1) Å, and c/a = 1.604 cell dimensions published in the literature.[20]

The XRD peak intensities of TcO_2 (Figure 2) exhibit a well-crystallized sample pattern. The Rietveld analysis on this XRD pattern was performed assuming a MoO_2-type monoclinic[8] unit cell with a $P2_1/c$ space group, and the lattice parameters were determined to be a = 5.6950 (3) Å, b = 4.7570(3) Å, c = 5.5234(5) Å, and β = 121.409(6)°. Previous study on TcO_2 by neutron powder diffraction[9] showed well-matched lattice parameters to these values. Furthermore, the XRD pattern did not show any impurities due to other crystalline-secondary phases.

3.2. Microscopic Analysis of the Samples. 3.2.1. Technetium Metal. The TEM BF image of the Tc metal in Figure 3a shows a round particle with a 414.5(5) nm diameter coming away from the bulk material. This particle consists of thickness contrast effects on the image, especially in the regions toward the bulk material due to the formation of particle clusters. However, the thin edges containing bright contrast show no precipitates or any other defects due to secondary phase contaminants. The area highlighted in the box was used to further study the phase purity of the particle by HRTEM imaging (Figure 4a), as the area has a streak across the particle. A comparison of the experimental SAD pattern (Figure 3b) with simulated SAD patterns showed that the zone axis of the images obtained is [001]. Figure 3c is a SAD simulation for Tc metal along the [100] direction with a camera length of 2000 mm. Other than the main diffractions, the experimental SAD pattern consists of faint diffraction spots and some ring patterns in the background. These faint-discrete spots which form few weak speckled patterns also indicate that the sample consists of large-sized grains. The thin carbon film on which the sample was mounted forms the faint ring patterns in the background of the SAD pattern.

The HRTEM image in Figure 4a, corresponding to the highlighted area of the TEM BF image in Figure 3a, comprises an interface forming two lattice fringe orientations. Further investigation showed that these two regions consist of lattice fringes with similar fringe spacing. It is concluded that this area is a twin boundary due to the overlapping of grains of the same chemical phase. Furthermore, the lattice fringe spacing matches the interplanar d spacing of the Tc

(19) Zuo, J. M.; Mabon, J. C. *Microsc. Microanal.* **2004**, *10* (Suppl. 2).

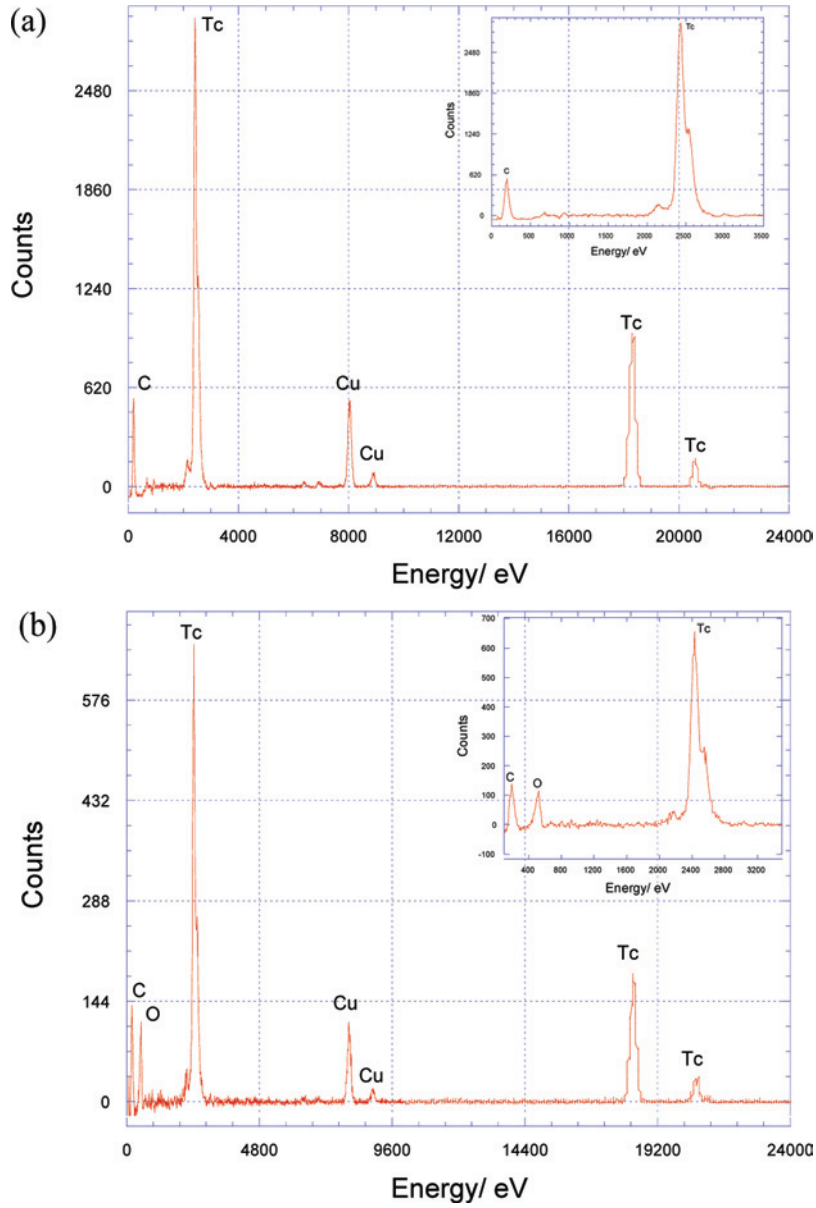

Figure 9. XEDS spectra of Tc (a) and TcO_2 (b). The insets to the upper-right of each plot are the magnified spectra to display the absence and presence of the oxygen peak in Tc metal and TcO_2, respectively. Carbon and Cu peaks are due to the sample mount made of a thin amorphous carbon film embedded on a copper grid.

Table 1. Elemental Distribution of TcO_2 Determined by XEDS and Theoretically

element	atomic %	uncertainty %	theoretical atomic %
O	27.247	0.275	24.632
Tc	72.752	1.312	75.367

metal in the [100] direction. Also, the grain boundary layer seems to have a uniform thickness, confirming the identical bonding and density characteristics throughout the observed particle. The HRTEM simulation present in Figure 4b was obtained along the [100] direction assuming a [001] beam direction. The fringe orientation of this image, similar to the experimental HRTEM image, confirms the lattice fringe formation along the [100] direction.

Another thin particle area without any grain boundaries was used to obtain the magnified HRTEM image shown in Figure 5a. The lattice fringes in this area also match with the (100) reflecting planes of Tc metal. The Bloch wave presentation of the HRTEM image along the [100] direction in the [001] beam direction is presented in Figure 5b. Lattice fringes with a high point resolution in the experimental HRTEM image match the calculated Bloch wave presentation along the assumed [100] direction, confirming the fringe formation along the same direction in Figure 5a. Spatial filling of the Tc atoms along the [100] plane in the Tc metal crystal structure is also modeled (Figure 5c). Estimation of the hexagonal Tc metal lattice parameters (Figure 5a) was accomplished by identifying the unit cell orientation along the [100] direction in Figure 5c. As shown in Figure 5a, these values were calculated within the limits of point resolution of the image.

3.2.2. Technetium Dioxide. Separated particles from the bulk area in Figure 6a show the platelike morphology of TcO_2. These particles indicate no inclusions of any impurity

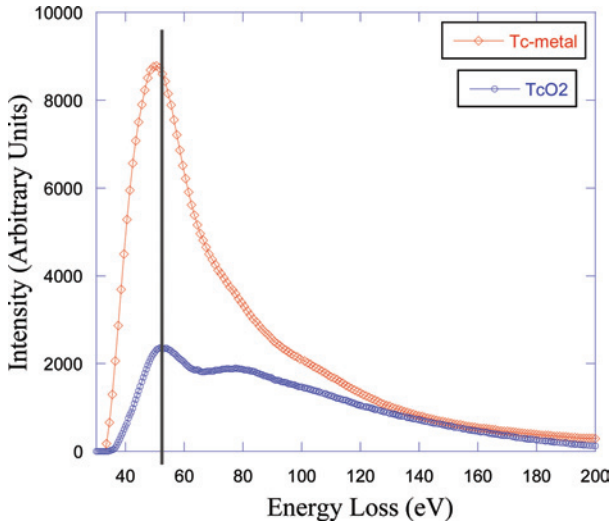

Figure 10. EELS low-loss spectra of Tc metal and TcO_2.

phases. As highlighted in Figure 6a with a box, a thin particle area of the sample was focused to obtain the HRTEM image shown in Figure 6b. There are two distinct areas in this HRTEM image. The lattice fringe details together with the corresponding fast Fourier transform indicate a presence of a grain boundary, as indicated in the image. The fringe spacing shows that the lattice fringes are due to systematic reflections of (−202) planes. A magnified HRTEM image (Figure 7) consists of lattice fringes along the same direction, [−202]. The lattice parameters of the TcO_2 crystal structure from the HRTEM image in Figure 7 were estimated to be $a = 0.501$ nm, $b = 0.427$ nm, and $c = 0.535$ nm. These values show significant differences (up to the second decimal point) compared to the values determined by XRD ($a = 0.5695$ nm, $b = 0.4757$ nm, and $c = 0.5523$ nm) due to the limited capability of the TEM technique and the complexity of the crystal system of TcO_2.

3.3. Microscopic Comparison of Tc and TcO_2. 3.3.1. Scanning Transmission Electron Microscopy. Tc metal and TcO_2 exhibit one crystalline chemical phase in each sample according to the XRD patterns and the TEM characterizations. TEM BF or HRTEM images for both of these materials showed no indication of any anomalous secondary phase inclusions or precipitates even though Tc metal (Figure 3a) and TcO_2 (Figure 6a) showed different morphologies. The TEM BF imaging of Tc showed that the sample consists of large agglomerated particles (Figure 3a), whereas TcO_2 particles are well-separated and crystallized. The Z-contrast STEM images (Figure 8) also confirm the morphological differences of the two samples. Tc metal (Figure 8a) has a larger particle size than TcO_2 (Figure 8b). TcO_2 particles have well-crystallized faces with a platelike shape, whereas Tc particles show no well-defined particular shape.

3.3.2. X-Ray Energy Dispersive Spectrometry. The XEDS spectrum of Tc metal (Figure 9a) shows no oxygen impurities, but the oxygen is prominent in TcO_2 (Figure 9b). XEDS is also used to quantify the elemental distribution of the TcO_2 sample, and the results are shown in Table 1. According to these results, an approximate stoichiometry of $TcO_{2.3}$ could be calculated within the uncertainties given in the Table 1.

3.3.3. Electron Energy-Loss Spectrometry. The Kramers−Kronig sum rule was used to calculate the absolute sample thicknesses based on the EELS spectra, and the values are 55.1 and 127.6 nm for Tc metal and TcO_2, respectively. The corresponding low-loss EELS spectra of Tc metal and TcO_2 samples are shown (Figure 10). A single peak was obtained for Tc metal, confirming that Tc is not a free-electron metal. However, there are two significant plasmon peaks at 50 and 80 eV in the TcO_2 low-loss spectrum, confirming greater thickness of the TcO_2 specimen than that of the Tc metal. The first peak is due to the Tc N_{23} edge, and the second weak peak is from the Tc N_1 edge. There is a small peak shift (2.0 eV) in the plasmon-loss spectra of these two compounds, confirming their distinctive bonding environments. The Tc N_{23} edge in the TcO_2 is shifted to a higher energy due to the strong ionic bonding in TcO_2 with respect to the Tc metal.

4. Discussion

XRD patterns of both samples showed that they are single-phased with respect to the crystalline chemical phases. The lattice parameters of the Tc metal sample were determined by XRD analysis ($a = 2.7431(3)$ Å, $c = 4.3989(5)$ Å) and estimated by HRTEM ($a = 0.284$ Å and $c = 0.454$ Å) imaging. Lattice parameters of TcO_2 estimated by HRTEM ($a = 0.501$ nm, $b = 0.427$ nm, $c = 0.535$ nm) also showed some differences to the values determined by XRD ($a = 0.5695$ nm, $b = 0.4757$ nm, and $c = 0.5523$ nm) similar to the Tc metal sample. The discrepancies between the lattice parameter values determined by XRD and HRTEM are likely due to the limited capability of the HRTEM technique to obtain high point resolution and the complexity of the crystal structures.

Both TEM BF and STEM imaging showed the presence of an agglomerated particle distribution in the Tc metal sample. Observation of these particle clusters implies a low crystallinity, which was also observed in XRD patterns, of the sample. Difficulty in obtaining well-resolved lattice fringes in the HRTEM images also verifies this behavior of Tc metal. Twin boundaries identified in HRTEM imaging could be due to an artifact generated from the sample preparation. On the other hand, high crystallinity of TcO_2 is prominent from both the XRD pattern and TEM imaging of the sample. TcO_2 particles with well-crystallized particle faces in TEM BF images revealed the monoclinic-like particle shape. Furthermore, a unique space-phase orientation of TcO_2 atomic units was detected with respect to the single crystals of its monoclinic unit cell from the HRTEM imaging. In addition, the 2-fold multiplicities of the fringes in two directions with long-range order of the atomic arrangement are also distinctive. Thus, the differences in morphology and point-

(20) Lam, D. J.; Darby, J. B.; Downey, J. W.; Norton, L. J. *Nature* **1961**, *192*, 744.

to-point resolution in the HRTEM imaging of these two samples could be related to the lack in crystallization or to the tendencies in forming divergent chemical phases with dissimilar chemical and physical characteristics.

XEDS spectra obtained for areas of Tc and TcO_2 did not reveal any impurities from the sample preparation. These spectra also showed that the Tc metal is oxygen-free. In the case of TcO_2, the stoichiometry of the two atoms could also be determined from the quantitative analysis of XEDS. EELS spectra were also useful in verifying the different bonding characteristics of these two samples, which have different chemical environmental properties. In comparing the plasmon peaks of Tc and TcO_2, a peak shift to a higher energy was detected in the Tc N_{23} edge for TcO_2, probably due to the strong ionic bonding in TcO_2 with respect to the Tc metal.

5. Conclusion

Transmission electron microscopy was utilized to characterize the morphology and the microstructure of Tc metal and TcO_2 synthesized by thermal decomposition of NH_4TcO_4. Single-phased characteristics of the samples were successfully confirmed by TEM techniques and X-ray powder diffraction patterns. The morphology of Tc metal showed significant differences compared to that of TcO_2. The crystal structure of Tc metal on the nanoscale was shown to contain well-resolved lattice fringes without any defects. Because of the deficiency in point resolution, however, the two-dimensional structure details of Tc metal could not be observed as expected. On the other hand, structural details of TcO_2 were prominent at high resolution. With a 2-fold multiplicity in both dimensions, TcO_2 showed a unique atomic distribution corresponding to monoclinic unit cell.

The stoichiometry of technetium dioxide was determined to be $TcO_{2.3}$ on the basis of the quantitative analysis of XEDS. Low-loss EELS measurements were performed, and the spectra confirmed the presence of Tc in both samples. A shift of 2.0 eV, to the lower end of the energy range, is noted in the Tc N_{23} edge when moving from TcO_2 to Tc metal due to different chemical environments.

Successful characterization of the ^{99}Tc-based samples by TEM suggests that these techniques can be extended to characterize other Tc metallic materials such as the Tc alloys (Tc−Zr and Tc−stainless steel) proposed for potential storage waste forms and the ε phase in nuclear fuel. Also, in corrosion experiments of Tc alloys, EELS and XEDS measurements can be performed to characterize products, such as in the case of the formation of TcO_2. In the context of transmutation of Tc into ruthenium and higher Z elements by neutron capture, TEM can support investigations into the structure defects by HRTEM and atomic distributions by EELS, providing information on the properties and behavior of resulting alloy materials.

Acknowledgment. The authors wish to thank Dr. Anthony Hechanova for administrating the UNLV Transmutation Research Program under the financial support of the U.S. Department of Energy (Grant No. DE-FG07-01AL67358). We also thank Dr. Clay Crow from the Department of Geoscience at UNLV, for helpful discussions and support. The authors are indebted to Tom O'dou and Trever Low for laboratory management and radiation safety.

IC8014628